

# Comparative Visualization of Multiple Time Surfaces by Planar Surface Reformation

Andrea Brambilla\*  
University of Bergen

Paolo Angelelli†  
University of Bergen

Øyvind Andreassen‡  
Norwegian Defence  
Research Establishment  
and University Graduate  
Center at Kjeller

Helwig Hauser§  
University of Bergen

## ABSTRACT

Comparing time surfaces at different integration time points, or from different seeding areas, can provide valuable insight into transport phenomena of fluid flows. Such a comparative study is challenging due to the often convoluted shapes of these surfaces. We propose a new approach for comparative flow visualization based on time surfaces, which exploits the idea of embedding the surfaces in a carefully designed, reformed 2D visualization space. Such an embedding enables new opportunities for comparative flow visualization. We present three different strategies for comparative flow visualization that take advantage of the reformation. By reforming the time surfaces, we not only mitigate occlusion issues, but we can devote also the third dimension of the visualization space to the comparative aspects of the visualization. Our approach is effective in a variety of flow study cases. The direct comparison of individual time surfaces reveals small scale differences and fine details about the fluid's motion. The concurrent study of multiple surface families enables the identification and the comparison of the most prominent motion patterns. This work was developed in close collaboration with an expert in fluid dynamics, who assessed the potential usefulness of this approach in his field.

**Index Terms:** I.3.3 [Computer Graphics]: Picture/Image Generation—Viewing algorithms

## 1 INTRODUCTION

In several application domains, including medicine and engineering, significant efforts are invested in analyzing the evolution of fluids over time. Studying the concurrent evolution of multiple particles has been shown to “increase the visual insight into flow structures encountered during their evolution” [21]. This type of analysis became popular in the fifties, thanks to dedicated experimental flow visualization methods, such as the tellurium method [44], the hydrogen bubble technique [15] or the spark discharge method [3]. These techniques provide temporal control for the release of a tracer along straight segments, allowing for the experimental production of time lines. Time lines are particularly useful in exposing the local profile of the flow velocity. Additionally, they emphasize local differences in flow dynamics over time in unsteady flows [28].

*Time surfaces* extend the effectiveness of time lines for studying fluid flows over three-dimensional domains. A time surface is defined as the surface that connects a set of particles simultaneously released into the flow from a two-dimensional seeding structure. This type of surface conveys the relative motion of the fluid over a

certain integration time. A set of consecutive time surfaces (a *family*) exposes the variation of the fluid's motion over the time interval. As time proceeds, the fluid particles are advected through the flow, and the shape of the time surface is transformed accordingly.

The visual inspection of a single time surface can only convey a limited amount of information. Studying multiple (families of) time surfaces, seeded across the spatio-temporal domain, provides a more comprehensive overview of the flow behavior. The investigation of several surfaces within a single family exposes details about the evolution of the fluid. The same holds for the analysis of datasets within an ensemble of simulations. In these scenarios, each time surface can be studied individually, but it is often more informative to determine and to observe the differences between the surfaces. Effective comparative visualization can be obtained, e.g., by side-by-side visualization or object-space juxtaposition [31, 16, 38]. In order to design an effective comparative visualization, the visual resources have to be carefully distributed between the entities being compared and the comparative aspects of the visualization. In the case of time surfaces, this task is particularly challenging. In fact, the effectiveness of the visual comparison is dependent on the user's ability to mentally relate the surfaces to each other. So, the available visual resources should be employed for supporting such a mental association. On the other hand, complex flow patterns can result in time surfaces with a high geometrical complexity. In order to extract information from a single convoluted surface, the user needs to explore multiple points of view. Occlusion problems are often addressed by clipping planes, and by finely tuned shading/transparency algorithms. Finding a suitable balance between the ease of comparison and the amount of information conveyed is crucial. The difficulty of the problem increases when studying and comparing entire families of surfaces.

The main contribution of our work is a novel visualization design for the comparison of time surfaces. The underlying idea is to reduce the geometric complexity of the surfaces by means of a planar reformation algorithm, in order to strengthen the comparative aspect of the visualization. This is achieved by embedding the time surfaces in a 2D space while preserving their informative content as much as possible. Visualizations in the reformed frame of reference are occlusion free, therefore proven visual comparison schemes, such as juxtaposition, superimposition and side-by-side visualization, can be directly applied. As an additional contribution, we describe three visualization strategies that we designed for exploiting the reformed visualization space at best. By facilitating the comparative visualization of flow data with respect to one or more families of time surfaces, our visualizations can provide an informative and expressive picture of flow phenomena. In this paper we focus on time surfaces, but our approach can be generalized to other kinds of surfaces, such as stream, path and streak surfaces.

## 2 BACKGROUND

This work involves concepts from surface reformation and from comparative, reformation-based, and flow visualization. Here, we give an overview of the related work in these areas.

\*e-mail: andrea.bram@gmail.com

†e-mail: Paolo.Angelelli@UiB.no

‡e-mail: oyvind.andreassen@ffi.no

§e-mail: Helwig.Hauser@UiB.no

## 2.1 Comparative visualization

Enabling the effective visual comparison of multiple entities is one of the main challenges in visualization. A comprehensive review of this topic was presented by Gleicher et al. [16], who also provided a meaningful categorization of comparative visualization designs. Pagendarm and Post [31] published a cornerstone work about comparative visualization in the early nineties. They classify comparative visualization methods into *image-level* (juxtaposition of images) and *data-level* techniques (placement of different visual entities in the same reference space). A third category, *feature-level* comparative visualization, was later introduced by Verma and Pang [38]. Further work has been published for the visual comparison of 2D data [35], 3D data [6] and polygonal meshes [7]. For flow visualization, Verma and Pang [38] introduced methods for the comparison of streamlines and streamribbons by object-space juxtaposition. Schlemmer et al. [34] instead focused on the feature-level comparison of 2D flows, using invariant moments as feature descriptors. Hummel et al. [19] proposed to use visual analysis tools, such as linking-and-brushing for the comparison of ensembles of CFD simulations. Angelelli and Hauser [1] proposed a method for straightening 3D tubular flow data (e.g., arterial blood flow) in order to facilitate image-level comparisons.

## 2.2 Surface reformation and 2D parameterization

The reformation of a surface to a planar domain can be reformulated as a 2D surface parameterization problem. This is a widely investigated research question in computer graphics [14, 36]. The general goal is to determine a one-to-one mapping (embedding) between a surface (triangular mesh) and a subset of the 2D Cartesian space. A classification can be defined according to which properties of the original surface are preserved. If angles are unchanged, we have a *conformal* mapping. The conformal mapping of a smooth surface is guaranteed to exist, is nearly unique, and can be computed efficiently [24]. An *authalic* parameterization preserves surface areas. Authalic mappings are not unique, so additional conditions (e.g., minimizing angle distortions) are usually taken into account [11]. A parameterization is *isometric* if the length of any arc on the surface is unchanged in the parameter space. For our purpose, an isometric reformation would be ideal, since it would introduce no deformation at all, but only a restricted set of surfaces allows an isometric embedding. The problem can be reformulated as an optimization. One possibility is to minimize a distortion metric based on lengths, angles and areas [33], but this approach usually requires extensive computations. Liu et al. [25] decompose the process into a local and a global optimization. Liu et al.'s algorithm can generate almost isometric (*as-rigid-as-possible*) mappings with performances comparable to state-of-the-art conformal mapping techniques. For these reason, we adopt this method for computing the reformation of time surfaces.

## 2.3 Reformation in visualization

Visualization literature is rich with techniques that employ reformation in order to provide a clearer, more complete, and simpler depiction of the data. Spatial transfer functions and generalized displacement mappings can be employed for warping the spatial domain of the phenomena of interest [9, 10]. Dedicated methods have been proposed for the reformation of tubular structures along a line. The so-called *curve-centric volume reformation* (CCVR) [23] straightens a 3D scalar field into a new volume centered around a 3D curve. Angelelli and Hauser [1] extended the CCVR in order to straighten tubular flow datasets, and to enable comparative visualization of flow data. Vilanova et al. [39] proposed a 2D reformation of the human colon, based on a non-linear radial raycasting from the colon's centerline. Straightening of the entire vascular tree can be obtained by the *curved surface reformation* [2]. Reformation is

exploited by Diepenbrock et al. [12] for improving the visual comparison of scans of small animals' blood vessels.

## 2.4 Flow visualization and integral structures

Integration-based flow visualization is concerned with the investigation of transport phenomena and long-term flow characteristics. The idea is to generate curves or surfaces by integrating the differential equation which describes the flow [27]. A *streamline* is a curve originating from a *seeding point* and everywhere tangent to the instantaneous flow field. A *path line* represents the trajectory of a particle released from a seeding point. A *streak line* emulates the continuous release of dye into a fluid. *Stream, path and streak surfaces* are obtained by densely seeding the respective type of integral lines from a given *seeding curve*. In contrast, a *time line* is the material line that connects a set of particles simultaneously released into the flow along a seeding curve. If particles are released from a *seeding surface*, we obtain a *time surface*. In this paper we focus on time surfaces, but extending our approach to other types of surfaces is straightforward.

The construction of stream and path surfaces in CFD datasets was already possible in the early nineties, while streak and time surfaces have been addressed only recently. The *smoke surfaces* by Von Funck et al. [41] is one of the first attempts to generate streak surfaces. The technique by Krishnan et al. [21] visualizes streak and time surfaces in real-time by exploiting a lengthy preprocessing phase. Thanks to parallel computation on the GPU, the construction of these type of surfaces can be performed in real-time as well [13]. Recently, Weinkauff et al. [43] describe a conceptual framework for treating any kind of integral structure in a unified way.

For convoluted surfaces, the problem of self-occlusion has been addressed with ad-hoc rendering styles. Born et al. [4] suggest to improve the visibility and the shape perception by means of contour lines, halftoning and transparency. Different strategies for controlling the transparency of the surfaces are presented by Hummel et al. [18] and Carnecky et al. [8].

The visualization of integral surfaces in a reformed 2D space has been recently investigated by Obermaier and Joy [30]. Their approach differs from ours in three important aspects. Because of the parameterization they adopt, all the reformed surfaces have a fixed square shape. The morphological information is therefore strongly compromised. We improve on this by adopting a reformation algorithm which preserves the original shape as much as possible. Additionally, while Obermaier and Joy focus on studying the deformation field only, we also enable the investigation of flow properties on the reformed surfaces. Finally, their approach is mainly concerned with the analysis and the rendering aspects of a single integral surface. In contrast, we present visualization strategies specifically designed for easing the comparison of multiple surfaces. In Section 9 we present and discuss a few visualizations obtained with the parameterization adopted by Obermaier and Joy.

## 3 METHOD'S OVERVIEW

Flow phenomena are often represented by 4D datasets, with three spatial dimensions and a temporal axis. The visual resources at our disposal are instead limited to the 2D space of standard display devices, plus the user's time (interaction and animations). These resources must be allocated in smart way in order to properly illustrate the flow phenomenon. This is particularly important for comparative visualization, since multiple pieces of information have to be presented in visual relation with each other. Our solution addresses this challenge by reducing the spatial complexity of the original datasets. On the one hand, we achieve a novel, simplified representation of the scenario under investigation. On the other hand, we exploit the thereby gained visual resources to strengthen the comparative visualization aspects of our solution.

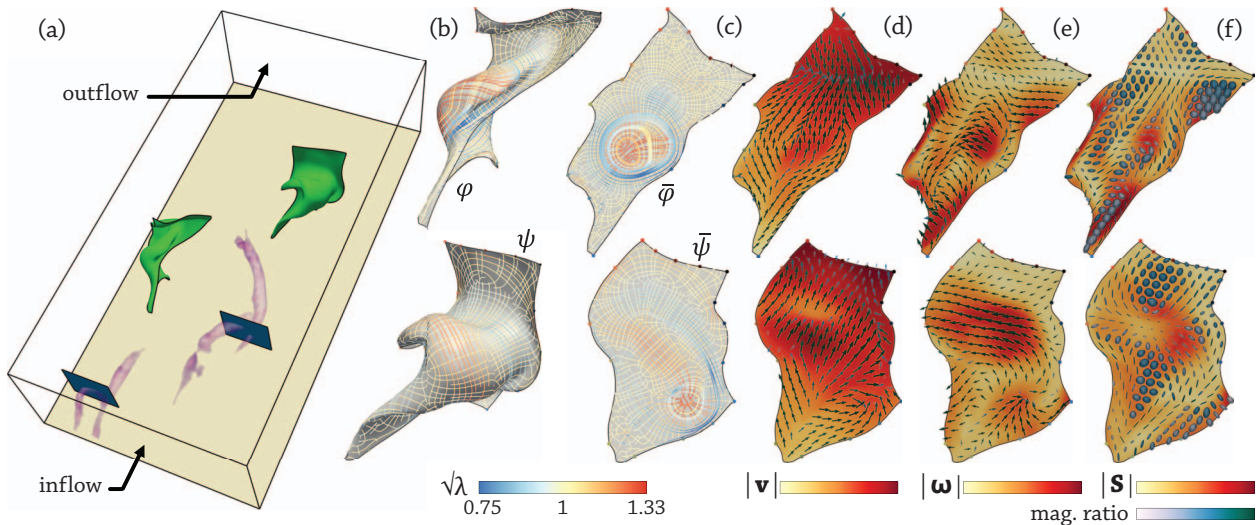


Figure 1: Visual comparison of two time surfaces using our new approach. Our analysis of this study case is described in Sec. 8. (a) The two time surfaces (green) in the turbulent channel dataset. The seeding planes (in blue) are placed in correspondence with a hairpin vortex (left) and two streamwise vortices (right), detected with the  $Q$  criterion [20] (in purple). (b, c) The original and the reformed surfaces with the tensor lines of the metric tensor field. The square roots of the related eigenvalues are mapped to colors in order to convey the local deformations. (d, e, f) Visualizations of the reformed velocity, vorticity and strain rate. The color of the surface encodes the magnitudes of the respective attribute, while the color of the glyphs depends on the alignment between the surface and the vectorial/tensorial quantity.

Our approach can be subdivided in two stages: a data reformation stage, executed as a pre-processing step, and an interactive comparative visualization stage. The input to the first stage is one or more families of time surfaces (Fig. 1ab, Fig. 3ac). We embed each of these surfaces in a two-dimensional space by exploiting the state-of-the-art parameterization algorithm by Liu et al. [25] (Fig. 1c). The benefits of the planar reformation are twofold. Firstly, such a representation mitigates occlusion issues, which normally interfere with the comparison process. Secondly, embedding the surfaces in a 2D space frees up the third dimension, which can then be exploited for comparative purposes [16]. Sections 3.1 and 3.2 are dedicated to the construction of time surfaces and to the reformation algorithm, respectively. In case the 3D surfaces to be compared are significantly different, their 2D reformations have dissimilar shapes as well. Establishing a visual relation between corresponding points in highly dissimilar 2D surfaces is challenging. In order to make this task easier, we provide orientation marks and interactive selection highlighting (Sec. 4).

Building on the new, reformed space, we present three specific visualization strategies that enable comparative flow visualization at different abstraction levels (Fig. 1, 3). We display the tensor lines of the *metric tensor field* on the reformed surfaces (Sec. 5), in order to provide information about the geometry of the original 3D surfaces. Coupling this kind of visualization with a side-by-side placement of multiple reformed surfaces enables the investigation of their morphological differences.

In our second visualization design, we enrich the visualization by depicting the scalar, vector and tensor fields over the reformed time surfaces (Sec. 6). We focus on the velocity, the vorticity and the rate of strain, but our approach can be applied to any other flow attribute. Vectorial and tensorial quantities have to be transformed according to the rules of *tensor calculus* in order to be displayed correctly in the reformed space. This approach lets the user investigate how the flow properties vary across multiple surfaces.

Both of these visualization approaches enable the comparison of two or more time surfaces by, e.g., side-by-side or flip-chart arrangements. Yet another strategy exploits the third spatial dimension for the surface comparison. We display an entire family of sur-

faces as a stack, ordered according to the integration time (Sec. 7). The user can specify an importance function over selected data attributes, which is then mapped to the opacity and color of the surfaces. The stack of surfaces conveys which time surfaces carry the important attribute values and how these values evolve over time. Additionally, a direct comparison of multiple families of surfaces can be carried out by juxtaposing the corresponding stacks along one axis of the screen.

Our visualization strategies require auxiliary pre-computations in addition to the surface reformation. The necessary data processing is presented together with the description of the related visualization strategies in the following sections. Notice that all of our visualizations run at interactive rates.

### 3.1 Time surfaces and surface integration

A time surface is the material surface that connects a set of particles simultaneously released into the flow from a set of seeding locations. More formally, let  $\varphi$  be a two-manifold, spatially and temporally located in the flow domain.  $\varphi$  is called the *seeding surface*. A time surface  $\varphi_\tau$  is a two-manifold obtained by advecting the seeding surface  $\varphi$  through the flow for an integration time  $\tau$ . Notice that  $\varphi_0 = \varphi$ . In practice, we adopt piecewise linear representations (triangular meshes) for both the seeding surface and the time surfaces.

With the expression *family* of time surfaces, we refer to a set of surfaces with a common seeding surface, ordered by increasing integration time. Often, the seeding surface is given as a planar mesh of rectangular shape. Here, we also adopt such a seeding geometry, but our approach can be easily adapted for handling any kind of seeding surface. The rectangular seeding geometry can be parameterized by a pair of parameters  $(s_0, s_1) \in [0, 1]^2$ .

Given a user-defined seeding structure, we adopt the approach by Krishnan et al. [21] to compute a family of time surfaces. The  $(s_0, s_1)$  parameters are associated with the vertices of the mesh, therefore they can be easily retained during the advection process. The parameter pair  $(s_0, s_1)$  define a bijective mapping between the surfaces in a family, so we exploit them for identifying matching points across the surfaces and across families of surfaces.

### 3.2 Surface reformation

For computing the planar surface reformation, we take advantage of the local/global 2D parameterization by Liu et al. [25]. This technique explicitly minimizes the amount of distortion introduced by the reformation process. Given a mesh  $\psi$ , we split it into triangles and embed them individually in 2D. The triangles' adjacency is ignored, so no deformation is introduced. The second step restores the initial mesh topology by transforming the triangles in the 2D space. The behavior of the reformation can be controlled by defining categories of *allowed transformations*. For instance, if only similarity transformations are allowed, the reformation corresponds to a conformal mapping. By limiting the set of allowed transformations to translations and rotations only, the desired as-rigid-as-possible reformation is achieved.

However, there is no guarantee that the original topology can be restored by applying a set of allowed transformations only. The idea is to employ a set  $L$  of transformations which are as similar as possible to allowed transformations. Given a point  $\mathbf{p} \in \psi$ , we denote with  $\mathbf{x} \in \mathbb{R}^2$  its initial embedded coordinates. Let  $\bar{\mathbf{p}} \in \bar{P} \subset \mathbb{R}^2$  be a set of points in the reformed space which is consistent with the topology of  $\psi$ . Finally, let  $L_t \in L$  be a transformation applied to triangle  $t \in T$ . The goal is to determine the sets  $(\bar{P}, L)$  that minimize the following energy function

$$\frac{1}{2} \sum_{t \in T} \sum_{(i,j) \in E_t} \cot(\theta_{ij}) \left\| (\bar{\mathbf{p}}_i - \bar{\mathbf{p}}_j) - L_t(\mathbf{x}_i - \mathbf{x}_j) \right\|^2 \quad (1)$$

where  $E_t$  are the three edges of triangle  $t$ , and  $\theta_{ij}$  is the angle opposite to the edge  $(i, j) \in E_t$  in the triangle  $t$ . The minimization process is iterative and includes a local and a global phase. At the first iteration, we initialize the points  $\bar{\mathbf{p}}$  according to their  $(s_0, s_1)$  parameter values. Equation 1 is then minimized with respect to  $L$ , taking only allowed transformations into account (local solution). The transformations from the local solution are substituted back into the equation, and we now minimize it with respect to  $\bar{P}$  (global solution). Local and global optimizations are alternated until the solution converges. The reformed surface  $\bar{\psi}$  is obtained by combining the final vertex positions  $\bar{\mathbf{p}}$  with the original mesh topology.

The whole process is “expected to be continuous” [37], therefore similar (consecutive) time surfaces are expected to have similar reformations. This has always been the case in our experiments. The chance to encounter discontinuities in the reformation process is remote, but if this would ever happen, a possible solution is to reseed a new family of time surfaces (Sec. 10).

### 4 ORIENTATION MARKS AND SELECTIONS

The reformation process maps 3D surfaces to a 2D space. Because of the introduced deformations, identifying where a given 3D point is placed in the reformed space (and vice versa) can be challenging. Similarly, when comparing multiple flattened surfaces, visually relating corresponding points can be problematic. We address this issue by providing orientation marks and interactive selections.

The  $(s_0, s_1)$  parameterization (Sec. 3.1) establishes a one-to-one correspondence between the 3D and the 2D surfaces. Moreover,  $(s_0, s_1)$  induces a mapping across families of time surfaces, assuming a one-to-one correspondence between the respective seeding geometries can be established. Orientation marks are colored dots distributed on the boundaries of the surfaces. We place them at regular intervals of the  $(s_0, s_1)$  parameterization (Fig. 2). Orientation marks have the advantage of not interfering with the visualization, but they convey only a limited amount of information. More details are provided on demand by interactive selections. We allow the user to interactively specify a location on a surface. The points with the same values of  $(s_0, s_1)$  are highlighted on all the other surfaces (2). Such a selection mechanism allows the user to get a clear idea of the correspondence between the surfaces being compared. Notice

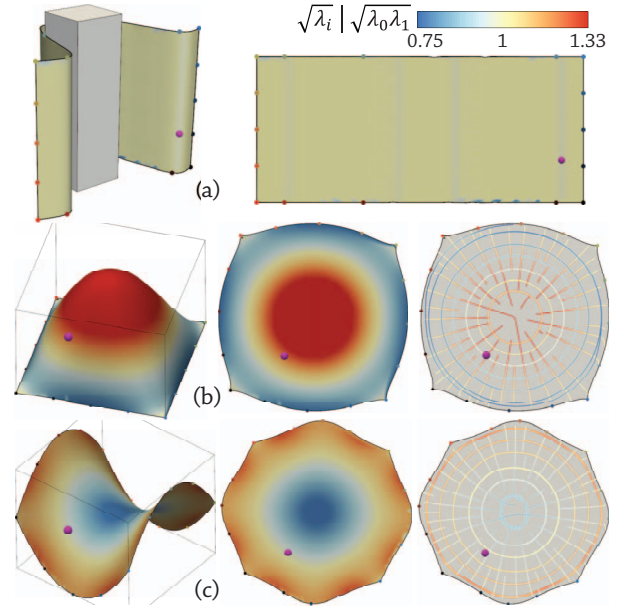


Figure 2: Examples of surface reformation. Orientation marks are displayed on the boundaries. The pink spheres indicate a user selected point and all the corresponding points across the surfaces. The surfaces are colored according to  $\sqrt{\lambda_0 \lambda_1}$ , using a logarithmic color scale (1st and 2nd columns). The same color scale is used for coloring the tensor lines, according to the square root of the respective eigenvalues (3rd column). (a) The surface can be reformed with almost no distortion,  $\sqrt{\lambda_0 \lambda_1}$  is close to 1 everywhere. (b) Colors indicate that the central region is compressed, while the outer regions are expanded. The tensor lines reveal that the deformation occurs mainly in the radial direction for the center, and in the tangential directions for the outer regions. (c) The surface is reformed by expanding the central region and compressing the outer regions. The tensor lines indicate that the deformation in the center is isotropic.

that selecting a point in a family of time surfaces highlights the path line passing through the selected point (Fig. 3bd).

### 5 SURFACE DEFORMATION ANALYSIS

The shape of a time surface encodes a fair amount of information about the flow behavior throughout the integration time. The morphological differences between time surfaces are a direct consequence of different patterns within the flow. For instance, a time surface traversing an area of strong rotational motion can become highly convoluted. In contrast, a surface traversing a strain dominated region is likely to increase its surface area while maintaining a relatively simple shape. In order to support an effective comparison of time surfaces, morphological information has to be represented in the reformed space.

The reformation algorithm (Sec.3.2) preserves the shape of the surface as much as possible, but in most cases local deformations are necessary for making the flattening possible. The direction and magnitude of one such deformation is encoded by a symmetric positive definite tensor called *metric tensor* (or *first fundamental form*), which is defined as follows [26]. Let  $\mathbf{p}$  be a point of a time surface  $\varphi$ , and  $\bar{\mathbf{p}}$  its corresponding point on the reformed surface  $\bar{\varphi}$ . Since  $\varphi$  and  $\bar{\varphi}$  are in a one-to-one correspondence,  $\mathbf{p}$  can be expressed as a function of  $\bar{\mathbf{p}}$ . We denote with  $\partial \mathbf{p} / \partial \bar{\mathbf{p}}$  the Jacobian matrix of this function. The metric tensor  $\mathbf{M}$  at point  $\bar{\mathbf{p}}$  is given by

$$\mathbf{M} = \left( \frac{\partial \mathbf{p}}{\partial \bar{\mathbf{p}}} \right)^T \frac{\partial \mathbf{p}}{\partial \bar{\mathbf{p}}}. \quad (2)$$

$\mathbf{M}$  depends on the specific location  $\bar{\mathbf{p}}$ . We compute  $\mathbf{M}$  for each point, therefore obtaining a tensor field over the reformed surface.

The metric tensor can be used to measure distances in the reformed space [26]. If we consider the distance

$$d\bar{r} = \|\bar{\mathbf{p}} - \bar{\mathbf{q}}\| = \sqrt{(\bar{\mathbf{p}} - \bar{\mathbf{q}})^T (\bar{\mathbf{p}} - \bar{\mathbf{q}})} \quad (3)$$

between two infinitesimally close points  $\bar{\mathbf{p}}, \bar{\mathbf{q}} \in \bar{\varphi}$ , the distance between  $\mathbf{p}, \mathbf{q} \in \varphi$  is given by

$$dr = \|\mathbf{p} - \mathbf{q}\| = \sqrt{(\bar{\mathbf{p}} - \bar{\mathbf{q}})^T \mathbf{M} (\bar{\mathbf{p}} - \bar{\mathbf{q}})}. \quad (4)$$

The metric tensor is symmetric and positive definite, so its spectral decomposition yields real eigenvalues  $\lambda_0, \lambda_1$  and orthogonal eigenvectors  $\mathbf{e}_0, \mathbf{e}_1$ . As a special case of Equation 4, if the vector  $\bar{\mathbf{p}} - \bar{\mathbf{q}}$  is aligned with the  $i$ -th eigenvector, we have

$$dr = \sqrt{(\bar{\mathbf{p}} - \bar{\mathbf{q}})^T \lambda_i (\bar{\mathbf{p}} - \bar{\mathbf{q}})} = d\bar{r} \sqrt{\lambda_i}. \quad (5)$$

Let  $dA \subset \varphi$  be an infinitesimal area on the 3D surface, and  $d\bar{A} \subset \bar{\varphi}$  the corresponding area in the reformed space. From Equation 5 it follows

$$dA = d\bar{A} \sqrt{\lambda_0 \lambda_1} = d\bar{A} \sqrt{\text{trace}(\mathbf{M})}. \quad (6)$$

A simple color coding of  $\sqrt{\lambda_0 \lambda_1}$  provides an overview of the deformations introduced by the reformation process (Fig. 2). If, at a point  $\mathbf{p}$ ,  $\varphi$  can be flattened without distortion, then  $\sqrt{\lambda_0 \lambda_1} = 1$ . In case  $0 < \sqrt{\lambda_0 \lambda_1} < 1$ ,  $dA$  is *expanded* by the reformation process ( $d\bar{A} > dA$ ). In contrast, if  $\sqrt{\lambda_0 \lambda_1} > 1$ , then  $dA$  is *compressed* ( $d\bar{A} < dA$ ).

The main directions of compression and expansion can be visualized through the field lines of the eigenvector fields (*tensor lines*). We convey the strength of the directional deformation along the  $\mathbf{e}_i$  tensor line by coloring the curve according to  $\sqrt{\lambda_i}$ . A value of  $0 < \sqrt{\lambda_i} < 1$  implies expansion along the tensor line, while  $\sqrt{\lambda_i} > 1$  indicates a compression. In order to deal with the ambiguous orientation of eigenvalues, we compute the tensor lines with the technique by Hotz et al. [17]. Notice that a logarithmic color scale is necessary in order to correctly represent the degree of compression and expansion.

The presented visualizations of the metric tensor field convey important information about the 3D geometry of the original surfaces. In particular, morphological differences between two or more surfaces can be identified by observing the shape and the tensor lines in the reformed space (Fig. 1c).

## 6 REFORMED FLOW ATTRIBUTES

In order to convey information about the local behavior of the flow, we visualize selected flow attributes on the reformed surfaces. We focus on the velocity, the vorticity and the strain rate fields, mainly because of their central role in fluid mechanics [40, 29], but our approach can be applied to any other scalar, vectorial and tensorial quantity. Given an infinitesimal fluid parcel in the domain, the velocity vector  $\mathbf{v}$  describes the instantaneous displacement of the parcel. The rotational motion of the parcel is described by the vorticity vector  $\boldsymbol{\omega} = \nabla \times \mathbf{v}$ . The strain rate tensor  $\mathbf{S} = 1/2 (\nabla \mathbf{v} + \nabla \mathbf{v}^T)$  encodes the instantaneous change of the shape and the volume of the parcel.

In order to enable an easy comparison of such attributes over multiple surfaces, we remap them (and their magnitudes) on the reformed surfaces. The magnitudes of these quantities are scalars, so they are invariant to the change of coordinate system induced by the surface reformation. In contrast, vectors and tensors include directional information which needs to be adjusted in order to be

represented correctly [26]. The reformation defines how to transform attributes that lie on the surface, but the ‘‘off-surface’’ (normal) component is ignored. Therefore, we have to first project the velocity, the vorticity and the strain rate onto the 3D surface. For each point of the surface  $\varphi$ , the projected attributes are

$$\mathbf{v}_\varphi = (\mathbf{I} - \mathbf{nn}^T) \mathbf{v} \quad (7)$$

$$\boldsymbol{\omega}_\varphi = (\mathbf{I} - \mathbf{nn}^T) \boldsymbol{\omega} \quad (8)$$

$$\mathbf{S}_\varphi = (\mathbf{I} - \mathbf{nn}^T) \mathbf{S} (\mathbf{I} - \mathbf{nn}^T)^T, \quad (9)$$

where  $\mathbf{n}$  is the surface normal at the current point. In order to compute their equivalent on the reformed surface  $\bar{\varphi}$ , we have to take into account the change of basis according to the rules of tensor calculus [26]. Velocity and vorticity behave as contravariant vectors and the strain rate as a mixed tensor. Therefore, we have

$$\mathbf{v}_{\bar{\varphi}} = (\partial \bar{\mathbf{p}} / \partial \mathbf{p}) \mathbf{v}_\varphi \quad (10)$$

$$\boldsymbol{\omega}_{\bar{\varphi}} = (\partial \bar{\mathbf{p}} / \partial \mathbf{p}) \boldsymbol{\omega}_\varphi \quad (11)$$

$$\mathbf{S}_{\bar{\varphi}} = (\partial \bar{\mathbf{p}} / \partial \mathbf{p}) \mathbf{S}_\varphi (\partial \mathbf{p} / \partial \bar{\mathbf{p}}), \quad (12)$$

where the matrix  $\partial \bar{\mathbf{p}} / \partial \mathbf{p}$  is the inverse of  $\partial \mathbf{p} / \partial \bar{\mathbf{p}}$  (Sec. 5).

On the reformed surface, the magnitude of each attribute can be visualized via color coding. The flattened velocity can be displayed using the common arrow glyphs (Fig. 1d). In this case, we scale the glyph according to the magnitude  $\|\mathbf{v}_{\bar{\varphi}}\| = \sqrt{(\mathbf{v}_{\bar{\varphi}})^T \mathbf{M} \mathbf{v}_{\bar{\varphi}}} = \|\mathbf{v}_\varphi\|$ . In order to convey the normal component that has been discarded by the reformation, we color the glyphs according to the ratio  $\|\mathbf{v}_{\bar{\varphi}}\| / \|\mathbf{v}\|$ , which can vary from 0 ( $\mathbf{v}$  orthogonal to  $\varphi$ ) to 1 ( $\mathbf{v}$  tangent to  $\varphi$ ). The same kind of visualization is provided for the vorticity (Fig. 1e). The strain rate is a symmetric tensor, therefore we employ ellipsoidal glyphs to visualize it (Fig. 1f). We scale a unit disk in the directions of the reformed eigenvectors of  $\mathbf{S}_{\bar{\varphi}}$ . The scaling in each direction is proportional to the respective eigenvalue of  $\mathbf{S}_{\bar{\varphi}}$ . Exponential scaling is adopted since the eigenvalues can be also negative [5]. The ellipsoids are colored according to magnitude ratio  $\|\mathbf{S}_{\bar{\varphi}}\| / \|\mathbf{S}\|$ .

For the sake of simplicity, we place the glyphs according to a regular hexagonal grid, but more advanced placement strategy can be easily plugged in.

## 7 STACKED SURFACES

The visualization strategies detailed so far are confined to the reformed 2D space. We can extend into a 3D visualization space and exploit the third dimension ( $z$ ) for supporting the comparative study of families of time surfaces. Given a set of reformed surfaces, we place them above each other, creating a stack (Fig. 3). Here we adopt the notation  $\bar{\varphi}^i$  for referring to the  $i$ -th surface in a family, in ascending order of integration time. We start by placing the first surface  $\bar{\varphi}^0 = \bar{\varphi}_0$  at the origin, with the normal aligned with the  $z$ -axis. The stack is created iteratively. The position and orientation of  $\bar{\varphi}^{i+1}$  in the  $xy$  plane is determined by minimizing (linear least squares) the distances between each point on  $\bar{\varphi}^{i+1}$  and the corresponding point on  $\bar{\varphi}^i$ . The displacement along the  $z$ -axis can be controlled by the user. Surfaces can also be inclined with respect to the  $z$ -axis. This makes them easier to study, but takes up more space in the third dimension. When the inclination angle reaches  $\pi/2$  the stack becomes a side-by-side visualization.

The user can freely navigate through a stack of surfaces, or even multiple stacks at the same time. We provide a focus+context visualization based on surface transparency. The user can select a scalar attribute of interest and interactively manipulate the transparency of the surfaces through an opacity transfer function. In this way, the user can immediately get an overview of the evolution of the selected property through a set of surfaces. Additionally, the user can

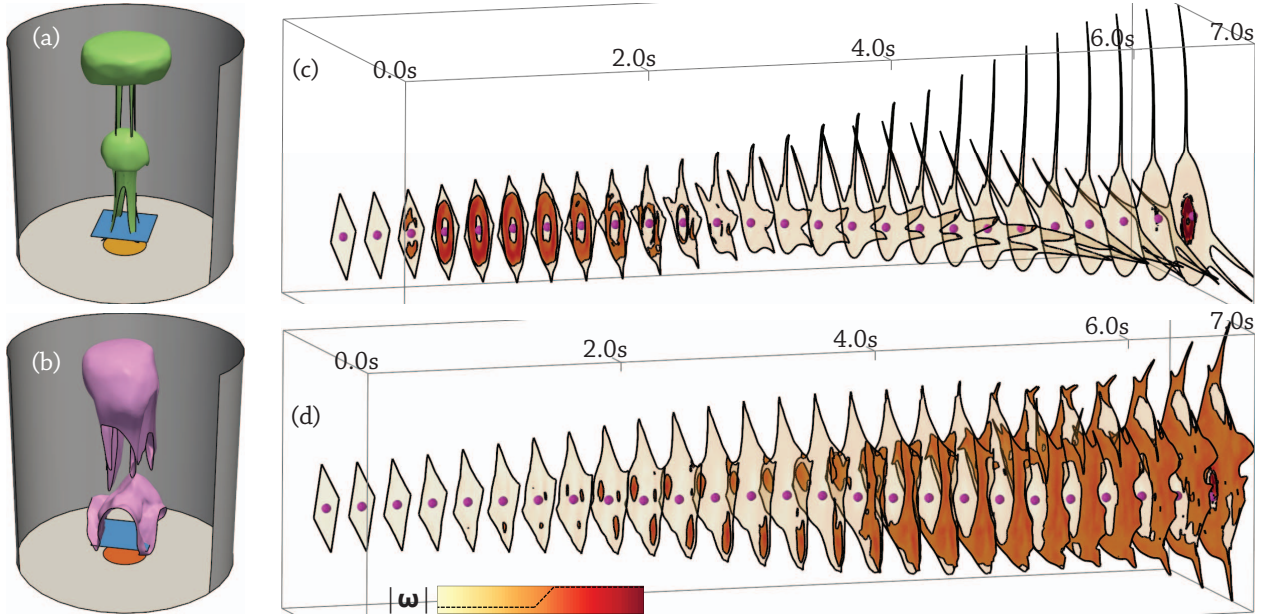


Figure 3: Two families of time surfaces in the heated cylinder dataset. (a, b) The 1st, 13th and 26th surface of each family. (c, d) Our stacked visualization strategy, where the transparency of the surfaces depends on the magnitude of the vorticity. The differences in the evolution of the vorticity across the two families are clearly exposed. The pink spheres indicate a manual selection (Sec.4).

observe how its evolution differs within multiple sets of time surfaces.

## 8 DEMONSTRATION

We showcase the capabilities of our technique by investigating selected families of time surfaces that we extracted from two different datasets. A third demonstration case is presented and discussed in the additional material. In our first application scenario, we compare time surfaces extracted from a direct numerical simulation of a statistically stationary flow in a turbulent channel [42] (Fig. 1a). Here, Taylor’s hypothesis [22] is nearly satisfied, meaning that the turbulent structures (eddies) change slowly over time. Therefore, the behaviour of such structures can be captured by series of time surfaces. We compute two families of time surfaces. The two seeding surfaces (in blue in Fig. 1a) are placed, respectively, in correspondence with a hairpin vortex and in-between two streamwise vortices, detected using the Q criterion [20] (in purple). We integrate the surfaces for  $0.1s$ , so that they cover a distance of about half of the channel’s length. We refer to the resulting surfaces as  $\varphi$  and  $\psi$  (Fig. 1b), and to the respective reformed surfaces as  $\bar{\varphi}$  and  $\bar{\psi}$  (Fig. 1c). By observing the tensor lines of the metric tensor field, we see that the reformation process introduced only small deformations in the top parts of the surfaces. This indicates that the flow in those areas is rather laminar. The distribution of the velocity vectors (Fig. 1d) and the low vorticity magnitudes are consistent with this interpretation. In the top part of  $\bar{\varphi}$  we see that there is an abrupt change in the direction of both velocity and vorticity, indicating the presence of a thin layer which moves faster than the surrounding area (shearing). The rate of strain (Fig. 1f) shows that the surface is stretched by this fast moving layer, especially in the area just below the layer.

Strong deformations are instead present in the bottom parts of  $\bar{\varphi}$  and  $\bar{\psi}$ . The distributions of the tensor lines indicate the presence of inflated regions in the original surfaces, analogously to the example in Figure 2b. In  $\bar{\varphi}$ , the  $e_1$  tensor lines are roughly aligned, meaning that the bulge has a larger extent in that direction, as can be seen in  $\varphi$ . To the lower left and to the right side of the bulge, the vorticity

and the velocity are aligned, which implies the presence of vortex cores in these areas, according to the *helicity* criteria [32]. These correspond to the two vortex legs of the initial hairpin vortex. The rate of strain is aligned with the cores, which is in agreement with the presence of streamwise vortices [40].

In  $\bar{\psi}$ , the amount of deformation around the bulge is approximately the same in every direction. The velocity and the vorticity exhibit patterns similar to swirling critical points, with large variations in orientation. This suggests the presence of a streamwise vortex orthogonal to the surface. The color of the ellipsoid glyphs reveals that the stretching in the normal direction is limited, indicating that the vortex and the time surface advance through the flow at approximately the same rate. Notice that performing a similar analysis in the original 3D space would have been highly challenging.

The second application scenario is a pair of simulations of the convective motion of air in a cylindrical chamber (Fig. 3ab). A heat source is located at the center of the base of the cylinder. The temperature of the heat source is set to  $100^\circ C$  in the first simulation, and to  $200^\circ C$  in the second one. We place the seeding surface slightly above the heat source. For each simulation, we compute a family of 26 time surfaces which covers a time period of  $7s$ , that is approximately the time needed for the time surfaces to reach the top of the cylinder. In order to compare the two different convective motions, we adopt our stacked visualization strategy, and we map the vorticity to the color and transparency of the surfaces. In the  $100^\circ C$  case (Fig. 3c), we see that areas of intense vorticity are traversed at an early integration time (between  $0.5s$  and  $3s$ ), corresponding to the initial ascension of the surface in the cylinder. At later times, vorticity appears to be low, while the deformation of the surfaces indicates a strain-dominated motion. In the  $200^\circ C$  case (Fig. 3d) instead, high magnitudes of vorticity are encountered at later integration times (around  $2s$ ), indicating that the time surface begins ascending in the cylinder later than in the previous case. This is quite counterintuitive, since we would expect the higher temperature to generate a faster convective motion. As a matter of fact, the high temperature also leads to the generation of turbulence in the first time steps of the simulation, before the convection becomes

predominant. The intense vorticity and the irregular shapes of the surfaces in the 200°C case represent the effects of turbulence during the early stages of the convective motion.

Further details about the flow behaviour can be obtained by studying the individual time surfaces. The clear advantage of the stacked visualization is that it enables the immediate identification of the main differences between the two cases.

## 9 THE $(s_0, s_1)$ PARAMETERIZATION

Two parameterization of time surfaces are exploited in our approach: the parameterization resulting from the reformation process, and the  $(s_0, s_1)$  parameterization. As a matter of fact, time surfaces can be visualized also in the 2D space given by  $(s_0, s_1)$ . This strategy has been adopted by Obermaier and Joy [30], who compute and visualize the metric tensor field with respect to  $(s_0, s_1)$ . Their goal is to realize illustrative rendering of individual surfaces. They exploit the metric tensor field for evenly distributing glyphs and tensor lines over the 3D surface, and for modulating the surface opacity.

In contrast, our goal is to ease the comparison of entire sets of time surfaces. In order to achieve this, we adopt a parameterization which reduces the geometrical complexity of the surfaces. The  $(s_0, s_1)$  parameterization is also effective in reducing the geometrical complexity, but it has the drawback that the morphological information is lost. Figures 4a and 4b respectively show the surfaces  $\varphi$  and  $\psi$  from Figure 1 reformed to the  $(s_0, s_1)$  space. The amount of deformation introduced, conveyed by color coding the eigenvalues of the metric tensor, is considerably larger than in Figure 1c. The reformed surfaces have exactly the same shape, so it may be easier for the user to mentally relate them to each other. However, it is practically impossible to identify, in the reformed space, any geometrical feature of the original 3D surfaces.

Figure 4c presents the same family of surfaces of Figure 3a adopting the  $(s_0, s_1)$  parameterization. The evolution of the vorticity is appropriately conveyed, but the spatial extent is inaccurate. By observing Figure 4c we can get the impression that the region of high vorticity magnitude rapidly expands after the 2nd surface, and shrinks abruptly after the 10th surface. In contrast, our visualization (Fig. 3c) clearly shows that expansion and shrinking are smooth and of limited extent. The issue is that the  $(s_0, s_1)$  parameterization is unable to capture the expansion of the time surface itself. Notice also that the peculiar shapes assumed by the time surfaces at late integration times are disregarded as well.

## 10 DISCUSSION

We discussed our approach with an expert from the CFD domain, who is also co-author of this paper. Our aim was to assess (a) the potential of our technique, (b) the best potential application scenarios, and (c) the advantages and disadvantages of our visualization strategies. Overall, the approach was deemed effective in simplifying the comparative analysis of time surfaces. The visualizations in the reformed space was considered useful for rapidly skimming through sets of time surfaces, eliminating the need for extensive user interaction in the early investigation phase. Complex motion patterns can lead to highly convoluted surfaces. So, it is often necessary to integrate time surfaces for only a short time, and seed new ones as soon as the geometry becomes too intricate. Our technique's ability to reduce the geometrical complexity enables the adoption of longer integration times. This means fewer reseeded steps, i.e., less manual work for the domain experts. The morphological information is partially lost, but the tensor lines of the metric tensor field are often sufficient for carrying out a preliminary analysis. A suggestion for improving this visualization strategy was to provide also curvature lines (curves tangent to the direction of the principal curvature) on the reformed surface. The reformation process also facilitates the comparison of flow attributes, which are im-

portant for identifying differences in the instantaneous flow behavior. Our visualization allows the user to quickly identify the main differences in the flow attributes across multiple surfaces. However, for a more thorough analysis, it can be convenient to have side-by-side visualizations depicting both the original and the reformed surfaces.

The stacked visualization is effective for producing an overview of one or more families of surfaces in a single picture. Besides identifying potentially interesting time surfaces, it can also steer the following steps of the analysis. For instance, an obstacle can be detected by looking for consecutive surfaces with zero velocity in corresponding regions. In that case, it can be reasonable to place a new seeding plane on each side of the obstacle. Or, if a set of time surfaces is found to traverse a vast turbulent area, one can consider to apply dedicated visualization techniques for studying that specific location.

## 11 CONCLUSION AND FUTURE WORK

We have presented a novel visualization solution that enables the comparative study of multiple families of time surfaces. To the best of our knowledge, this is the first visualization approach that enables the simultaneous analysis and comparison of a large number of time surfaces. Our approach exploits a planar reformation technique for reducing the geometric complexity of the original data. Comparative visualization is achieved at different levels of abstraction by employing appropriately designed visualization strategies. Our techniques can be also combined for investigating complex flow data. Surface stacks reveal different flow patterns within the surface families and highlight the interesting time surfaces. The selected surfaces can be compared according to flow characteristics or morphological properties.

We see several opportunities for extending our framework. First, the application of our technique to other kinds of integral surfaces seems to be straightforward. Second, each visualization strategy can be improved in different ways. For instance, other flow properties (e.g., pressure and stress) can be included. The reformation algorithm can be easily modified in order to include a user specified importance measure. In this way the deformation would be concentrated in unimportant regions, while the relevant areas would preserve their shape as much as possible. Furthermore, we can exploit our parameterization for distributing glyphs on the surfaces. Compared to Obermayer and Joy [30], we expect our approach to produce more uniform distributions in areas where the  $(s_0, s_1)$  parameterization would introduce large distortions

## REFERENCES

- [1] P. Angelelli and H. Hauser. Straightening tubular flow for side-by-side visualization. *IEEE Trans. on Visualization and Computer Graphics*, 17(12):2063–2070, 2011.
- [2] T. Auzinger, G. Mistelbauer, I. Baclija, R. Scherthaner, A. Köchl, M. Wimmer, M. E. Gröller, and S. Bruckner. Vessel visualization using curved surface reformation. *IEEE Trans. on Visualization and Computer Graphics*, 19(12):2858–2867, 2013.
- [3] H. J. Bomelburg, J. Herzog, and J. R. Weske. The electric spark method for quantitative measurements in flowing gases. Technical report, Maryland. Univ., College Park. Inst. for Fluid Dynamics and Applied Mathematics, 1959.
- [4] S. Born, A. Wiebel, J. Friedrich, G. Scheuermann, and D. Bartz. Illustrative stream surfaces. *IEEE Trans. on Visualization and Computer Graphics*, 16:1329–1338, 2010.
- [5] A. Brambilla, Ø. Andreassen, and H. Hauser. Integrated multi-aspect visualization of 3D fluid flows. In *Proc. 18th Workshop on Vision, Modeling and Visualization*, pages 1–9, 2013.
- [6] S. Bruckner and T. Möller. Result-driven exploration of simulation parameter spaces for visual effects design. *IEEE Trans. on Visualization and Computer Graphics*, 16(6):1468–1476, 2010.

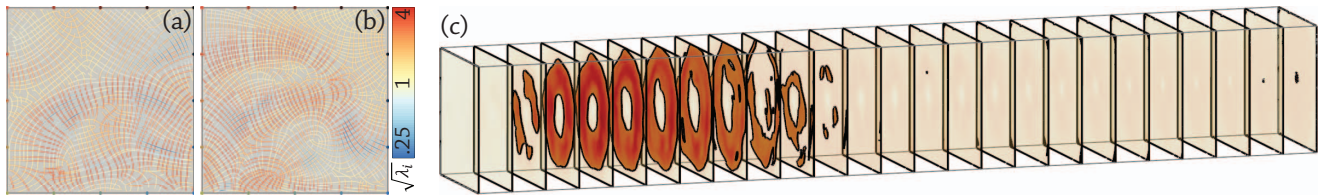


Figure 4: Results obtained by adopting the  $(s_0, s_1)$  parameterization. (a, b) Surfaces  $\phi$  and  $\psi$  from Fig. 1. (c) Surface family from Fig. 3ac.

- [7] S. Busking, C. P. Botha, L. Ferrarini, J. Milles, and F. H. Post. Image-based rendering of intersecting surfaces for dynamic comparative visualization. *The Visual Computer*, 27(5):347–363, 2011.
- [8] R. Carnecky, R. Fuchs, S. Mehl, Y. Jang, and R. Peikert. Smart transparency for illustrative visualization of complex flow surfaces. *IEEE Trans. on Visualization and Computer Graphics*, 19(5):838–851, 2013.
- [9] M. Chen, D. Silver, A. S. Winter, V. Singh, and N. Cornea. Spatial transfer functions: a unified approach to specifying deformation in volume modeling and animation. In *Proc. 2003 Eurographics/IEEE TVCG Workshop on Volume graphics*, pages 35–44. ACM, 2003.
- [10] C. D. Correa, D. Silver, and M. Chen. Discontinuous displacement mapping for volume graphics. In *Proc. Volume Graphics*, volume 6, pages 9–16, 2006.
- [11] P. Degener, J. Meseth, and R. Klein. An adaptable surface parameterization method. In *Proceedings, 12th International Meshing Roundtable*, pages 201–213, 2003.
- [12] S. Diepenbrock, S. Hermann, M. Schäfers, M. Kuhlmann, and K. Hinrichs. Comparative visualization of tracer uptake in in vivo small animal PET/CT imaging of the carotid arteries. In *Computer Graphics Forum*, volume 32, pages 241–250. Wiley Online Library, 2013.
- [13] F. Ferstl, K. Bürger, H. Theisel, and R. Westermann. Interactive separating streak surfaces. *IEEE Trans. on Visualization and Computer Graphics*, 16(6):1569–1577, 2010.
- [14] M. S. Floater and K. Hormann. Surface parameterization: a tutorial and survey. In *Advances in Multiresolution for Geometric Modelling*, pages 157–186. Springer Berlin Heidelberg, 2005.
- [15] E. W. Geller. An electrochemical method of visualizing the boundary layer. *Journal of the Aeronautical Sciences*, 22(12):869–870, 1955.
- [16] M. Gleicher, D. Albers, R. Walker, I. Jusufi, C. D. Hansen, and J. C. Roberts. Visual comparison for information visualization. *Information Visualization*, 10(4):289–309, 2011.
- [17] I. Hotz, J. Sreevalsan-Nair, H. Hagen, and B. Hamann. Tensor field reconstruction based on eigenvector and eigenvalue interpolation. In *Scientific Visualization: Advanced Concepts*, volume 1, pages 110–123. Schloss Dagstuhl–Leibniz-Zentrum fuer Informatik, 2010.
- [18] M. Hummel, C. Garth, B. Hamann, H. Hagen, and K. I. Joy. IRIS: Illustrative rendering for integral surfaces. *IEEE Trans. on Visualization and Computer Graphics*, 16:1319–1328, 2010.
- [19] M. Hummel, H. Obermaier, C. Garth, and K. I. Joy. Comparative visual analysis of Lagrangian transport in CFD ensembles. *IEEE Trans. on Visualization and Computer Graphics*, 19(12):2743–2752, 2013.
- [20] J. C. R. Hunt, A. A. Wray, and P. Moin. Eddies, streams, and convergence zones in turbulent flows. In *Studying Turbulence Using Numerical Simulation Databases*, 2, pages 193–208, 1988.
- [21] H. Krishnan, C. Garth, and K. Joy. Time and streak surfaces for flow visualization in large time-varying data sets. *IEEE Trans. on Visualization and Computer Graphics*, 15(6):1267–1274, 2009.
- [22] P. K. Kundu and I. M. Cohen. *Fluid Mechanics*. Academic Press, 2008.
- [23] O. D. Lampe, C. Correa, K.-L. Ma, and H. Hauser. Curve-centric volume reformation for comparative visualization. *IEEE Trans. on Visualization and Computer Graphics*, 15(6):1235–1242, 2009.
- [24] B. Lévy, S. Petitjean, N. Ray, and J. Maillot. Least squares conformal maps for automatic texture atlas generation. *ACM Trans. on Graphics*, 21(3):362–371, 2002.
- [25] L. Liu, L. Zhang, Y. Xu, C. Gotsman, and S. J. Gortler. A local/global approach to mesh parameterization. *Computer Graphics Forum*, 27(5):1495–1504, 2008.
- [26] D. Lovelock and H. Rund. *Tensors, differential forms, and variational principles*. Dover, 1989.
- [27] T. McLoughlin, R. S. Laramée, R. Peikert, F. H. Post, and M. Chen. Over two decades of integration-based, geometric flow visualization. *Computer Graphics Forum*, 29(6):1807–1829, 2010.
- [28] W. Merzkirch. *Flow Visualization, 2nd ed.* Academic Press, 1987.
- [29] K. K. Nomura and G. K. Post. The structure and dynamics of vorticity and rate of strain in incompressible homogeneous turbulence. *Journal of Fluid Mechanics*, 377:65–97, 1998.
- [30] H. Obermaier and K. I. Joy. Derived metric tensors for flow surface visualization. *IEEE Trans. on Visualization and Computer Graphics*, 18(12):2149–2158, 2012.
- [31] H.-G. Pagendarm and F. H. Post. Comparative visualization - approaches and examples. In *Visualization in Scientific Computing*, pages 95–108, 1995.
- [32] R. Peikert and M. Roth. The “parallel vectors” operator: a vector field visualization primitive. In *Proc. IEEE Visualization '99*, pages 263–270, 1999.
- [33] P. V. Sander, J. Snyder, S. J. Gortler, and H. Hoppe. Texture mapping progressive meshes. In *Proc. 28th Int'l Conf. on Computer Graphics and Interactive Techniques*, pages 409–416. ACM, 2001.
- [34] M. Schlemmer, I. Hotz, B. Hamann, and H. Hagen. Comparative visualization of two-dimensional flow data using moment invariants. In *VMV*, pages 255–264, 2009.
- [35] J. Schmidt, E. Gröller, and S. Bruckner. VAICo: Visual analysis for image comparison. *IEEE Trans. on Visualization and Computer Graphics*, 19(12):2090–2099, 2013.
- [36] A. Sheffer, E. Praun, and K. Rose. Mesh parameterization methods and their applications. *Foundations and Trends in Computer Graphics and Vision*, 2(2):105–171, 2006.
- [37] O. Sorkine and M. Alexa. As-rigid-as-possible surface modeling. In *Proc. 5th Eurographics Symposium on Geometry Processing*, pages 109–116. Eurographics Association, 2007.
- [38] V. Verma and A. Pang. Comparative flow visualization. *IEEE Trans. on Visualization and Computer Graphics*, 10(6):609–624, 2004.
- [39] A. Vilanova, E. Gröller, and A. König. Cylindrical approximation of tubular organs for virtual endoscopy. In *Proc. Computer Graphics and Imaging*, volume 11, pages 283–289, 2000.
- [40] A. Vincent and M. Meneguzzi. The spatial structure and statistical properties of homogeneous turbulence. *Journal of Fluid Mechanics*, 225:1–20, 1991.
- [41] W. von Funck, T. Weinkauff, H. Theisel, and H.-P. Seidel. Smoke surfaces: An interactive flow visualization technique inspired by real-world flow experiments. *IEEE Trans. on Visualization and Computer Graphics*, 14(6):1396–1403, 2008.
- [42] C. E. Wasberg, T. Gjesdal, B. A. P. Reif, and Ø. Andreassen. Variational multiscale turbulence modelling in a high order spectral element method. *Journal of Computational Physics*, 228(19):7333–7356, 2009.
- [43] T. Weinkauff, H.-C. Hege, and H. Theisel. Advected tangent curves: A general scheme for characteristic curves of flow fields. *Computer Graphics Forum*, 31(2):825–834, 2012.
- [44] F. X. Wortmann. A method of observation and measurement of the flow of water with tellurium. *Zeitschrift fuer Angewandte Physik*, 5:201–206, 1953.